



Downregulated UCHL1 Accelerates Gentamicin-Induced Auditory Cell Death via Autophagy

Yeon Ju Kim¹ · Kyung Kim² · Yun Yeong Lee¹ · Oak-Sung Choo^{1,3} · Jeong Hun Jang¹ · Yun-Hoon Choung^{1,3,4}

Received: 13 August 2018 / Accepted: 2 April 2019
© Springer Science+Business Media, LLC, part of Springer Nature 2019

Abstract

The clinical use of aminoglycoside antibiotics is partly limited by their ototoxicity. The pathogenesis of aminoglycoside-induced ototoxicity still remains unknown. Here, RNA-sequencing was conducted to identify differentially expressed genes in rat cochlear organotypic cultures treated with gentamicin (GM), and 232 and 43 genes were commonly up- and downregulated, respectively, at day 1 and 2 after exposure. Ubiquitin carboxyl-terminal hydrolase isozyme L1 (*Uchl1*) was one of the downregulated genes whose expression was prominent in spiral ganglion cells (SGCs), lateral walls, as well as efferent nerve terminal and nerve fibers. We further investigated if a deficit of *Uchl1* in organotypic cochlea and the House Ear Institute-Organ of Corti 1 (HEI-OC1) cells accelerates ototoxicity. We found that a deficit in *Uchl1* accelerated GM-induced ototoxicity by showing a decreased number of SGCs and nerve fibers in organotypic cochlear cultures and HEI-OC1 cells. Furthermore, *Uchl1*-depleted HEI-OC1 cells revealed an increased number of autophagosomes accompanied by decreased lysosomal fusion. These data indicate that the downregulation of *Uchl1* following GM treatment is deleterious to auditory cell survival, which results from the impaired autophagic flux. Our results provide evidence that UCHL1-dependent autophagic flux may have a potential as an otoprotective target for the treatment of GM-induced auditory cell death.

Keywords Aminoglycoside · Autophagic flux · Ototoxicity · RNA-sequencing · UCHL1

Introduction

Gentamicin (GM) is still one of the most widely used aminoglycoside antibiotics for the treatment of various bacterial

Electronic supplementary material The online version of this article (<https://doi.org/10.1007/s12035-019-1598-y>) contains supplementary material, which is available to authorized users.

✉ Yun-Hoon Choung
yhc@ajou.ac.kr

¹ Department of Otolaryngology, Ajou University School of Medicine, San 5 Woncheon-dong, Yeongtong-gu, Suwon 443-721, Republic of Korea

² Division of Hematology-Oncology, Department of Medicine, Samsung Medical Center, Sungkyunkwan University School of Medicine, Seoul, Republic of Korea

³ Department of Medical Sciences, Ajou University Graduate School of Medicine, San 5 Woncheon-dong, Yeongtong-gu, Suwon 443-721, Republic of Korea

⁴ BK21 Plus Research Center for Biomedical Sciences, Ajou University Graduate School of Medicine, San 5 Woncheon-dong, Yeongtong-gu, Suwon 443-721, Republic of Korea

infections. However, aminoglycosides can also cause adverse effects such as ototoxicity [1] and nephrotoxicity [2]. In particular, ototoxicity has been reported to occur in about 2–25% of patients treated with aminoglycosides [3], and has been shown to have irreversible and permanent characteristics. In addition, the onset of symptoms may not be observed during the acute phase, and may be delayed for days or months [4]. Despite the delayed symptoms, GM seems to rapidly enter the sensory hair cells (HCs) via endocytosis on the apical membrane, basolateral membrane [5, 6], or mechanoelectrical transducer (MET) channel located at the top of HC stereocilia [6]. Earlier studies demonstrated that labeled GM started to increase 1 h after systemic injection in the organ of Corti, and was detected in the HCs after 3 h [7].

GM, a strong cationic drug, is taken up into sensory HCs through receptor-mediated endocytosis forming complexes with iron. This GM-iron complex catalyzes the oxidation, thereby inducing formation of reactive oxygen species [8] and activates c-Jun N-terminal kinase, which in turn induces apoptosis. The endocytosis of GM has been identified by the appearances of the vesicles in the subcuticular region and cytoplasm of HCs [5, 9], especially with the cationic ferritin observed in the vesicle

membrane [5]. In the HCs, denser, more heterogeneous, and more pleomorphic lysosomes are also induced. Cytoplasmic vacuoles in the spiral ganglion cells (SGCs) also increased with increasing GM concentration. However, it is not clear whether these lysosomal characteristics are the result of active pinocytosis or phagocytosis or autophagy [10].

Our previous study showed an increased number of autophagic vacuoles in HCs following systemic administration of GM, and reported that autophagic flux participated in the mechanism of delayed GM-induced ototoxicity [11]. However, the molecular mechanism underlying this is not fully understood.

In the past, GM was thought to be preferentially taken up by HCs in the cochlea. Therefore, death of SGCs was considered to be a secondary effect of downstream damage by GM-induced HC death. However, a few recent studies have suggested that SGCs can be directly affected by aminoglycoside without HC loss. For example, in the chinchilla inner ear, SGCs were found to have high levels of GM [12], and direct protection of these cells has alleviated the GM-induced hearing loss [13, 14].

In the present study, we have attempted to discover novel genes related to the pathogenesis of GM using the entire length of the organ of Corti and SGCs. High-throughput RNA sequencing (RNA-seq) and bioinformatics technologies were applied to characterize differences in levels of gene transcription between GM-treated and untreated cochlear explants. The objectives of this study were to identify differentially expressed genes (DEGs) in the cochlea tissues in the presence and absence of GM, to discover the novel protein interaction network modules related with the pathogenesis of GM treatment, to identify the distribution of proteins encoded by the DEGs, and to provide a functional relationship between the identified proteins and GM treatment.

Materials and Methods

Cochlear Organotypic Culture

All animal procedures were approved by the institutional review board of the Ajou University School of Medicine (AJIRB-MED-SMP-11-002). Sprague-Dawley rats (SD-rat, Daehan Bio-link, Cheongju, Korea) were decapitated on postnatal day 7. The cochlea was carefully removed, the lateral wall was dissected away, and the organs of Corti containing the entire basilar membrane and SGCs were placed in a tissue culture plate. Explants were maintained in Dulbecco's modified Eagle medium (DMEM; Gibco-BRL, Grand Island, NY, USA) including 10% fetal bovine serum (FBS; Gibco-BRL) and 0.06 mg/ml penicillin (Sigma-Aldrich, Steinheim, Germany) at 37 °C with 5% CO₂. The next day, a total of 24 cochleae were randomly divided into 3 groups ($n=8$ per group), and medium was exchanged with or without 50 μM GM (Sigma-Aldrich).

RNA Isolation and Sequencing

Total RNA was extracted from eight cochlear explants on days 1 and 2 after GM or DW treatment using the RNAPrep Pure Kit for tissue (Tiangen Biotech, Beijing, China) according to the manufacturer's instructions. Preparation of the RNA library and sequencing were performed by Macrogen (Seoul, Korea). To construct cDNA libraries with the TruSeq RNA library kit, 1 μg of total RNA was used. The protocol consisted of polyA-selected RNA extraction, RNA fragmentation, random hexamer primed reverse transcription, and 100 nucleotide (nt) paired-end sequencing by Illumina HiSeq2000 (Illumina, San Diego, CA, USA). The libraries were quantified using qPCR according to the qPCR Quantification Protocol Guide (Illumina), and qualified using an Agilent Technologies 2100 Bioanalyzer (Agilent Technologies, Santa Clara, CA, USA).

To estimate expression levels and to identify alternatively spliced transcripts, the RNA-seq reads were mapped to the genome of mouse or *Drosophila melanogaster* using TopHat [15], which is capable of reporting split-read alignments across splice junctions and determined using Cufflinks software [16] with default options. The reference genome sequence of rat (*Rattus norvegicus* [rn4]) and annotation data were downloaded from the University of California, Santa Cruz website (<http://genome.ucsc.edu>). The transcript counts at the isoform level and gene level were calculated, and the relative transcript abundances were measured in FPKM (fragments per kilobase of exon per million fragments mapped) using Cufflinks.

Gene Ontology Term Enrichment Analysis

Gene functional annotation analysis for the DEG list was performed using the Database for annotation, visualization, and integrated discovery (DAVID) tool (<http://david.abcc.ncifcrf.gov/>) [17] to understand biological meanings behind a large list of genes. The DAVID tool provides the functional annotation for over 40 annotation categories, including gene ontology (GO) terms, protein-protein interactions, protein functional domains, disease associations, bio-pathways, general sequence features, homologies, gene functional summaries, gene tissue expressions, and literatures.

In the DAVID annotation system, modified Fisher Exact p value (EASE score) was adopted to measure the gene-enrichment in annotation terms. If the EASE Score was lower than 0.05 for the specific GO-term, the given gene list is specifically associated with the GO term more than random chance. All data analysis and visualization of differentially expressed genes was conducted using R 3.0.2 (www.r-project.org).

Hierarchical Clustering

Hierarchical clustering analysis was performed using complete linkage and Euclidean distance as a measure of similarity to display the expression patterns of DEGs, which are satisfied with a fold change ≥ 1.5 and raw p value < 0.05 in the independent t test.

Analysis of the Protein-Protein Interaction Network

For human protein–protein interaction networks, we compiled data from well-known open databases, including HPRD [18], BioGRID [19], IntAct [20], MINT [21], Reactome [22], iRefWeb, [23] as well as the previous result of Lee et al. [24]. A total of 136,489 interactions among 14,216 human proteins were prepared. To identify and visualize the GM-induced auditory cell death-related protein network modules, we used Cytoscape [25]. The Molecular Complex Detection (MCODE) plugin of Cytoscape [26] was used to find highly interconnected regions in a protein-protein interaction (PPI) network, which are known as the hubs.

Quantitative Reverse-Transcriptase Polymerase Chain Reaction

Total cochlear RNA was extracted with the RNA prep pure tissue kit (Tiangen Biotech) according to the manufacturer's instructions. Standard RT was performed with the amfiRivert cDNA Synthesis kit (GenDEPOT, Barker, TX, USA) according to the manufacturer's instructions. Quantitative reverse-transcriptase polymerase chain reaction (qRT-PCR) measurements were performed using the ABI Prism 7000 Sequence Detection System (Applied Biosystems, Foster City, CA, USA) and a SYBR Green I qPCR kit (Takara, Otsu, Japan) according to the manufacturer's instructions. The cDNA was amplified with the following primers: 5'-CCCC GAAGATAGAGCCAAG-3' and 5'-ATGGTTCACTGGAA AGGG-3' for rat *Uchl1* B; 5'-ACAAGGCTCTGAGT GACCACCATG-3' and 5'-ACGGTTGCCATGGCAATTTC CTC-3' for rat *Kif5b*; 5'-ACCTGCCTCCTCAGATAAG-3' and 5'-ACTGAGAAGCTGTCTGCTG-3' for rat *CPNE3*; 5'-AGTCCGAGGCCACTGTCAATGTG-3' and 5'-CGGC CTTTGTTCCAGATG-3' for rat *Ncam1*; 5'-TTGC GGGTCTTGACATGAAT-3' and 5'-AACTTGTGGCGGTG TCCATA-3' for rat *Tnks*; 5'-CCGGCTGATTGAGTCCCTC-3' and 5'-CCCCGATGTCGTAATTCTGG-3' for mouse *Sqstm1/p62*; 5'-GGTTGCAGGGCTTCGAGAAGCAG-3' and 5'-GCTTCCCCTTCATACCACACC-3' for rat *Gusb*; and 5'-AACGGGAAGCCCCATCACCC-3' and 5'-CAGC CTTGGCAGCACCAG-3' for mouse *Gapdh*. Normalizing to *Gusb* and *Gapdh*, the relative gene expression was analyzed by the comparative threshold cycle (CT) method (Applied Biosystems). The Ct values of the reference genes were

around 20–25, and were consistent across all biological replicates. *Gusb* and *Gapdh* were used as the reference genes for the rat organ of Corti due to their stable expression [27, 28]. The expression of the genes of interest was expressed as fold change over the control.

Cell Culture and Transfection

House Ear Institute-organ of Corti 1 (HEI-OC1) cells were grown in DMEM (Gibco-BRL, Grand Island, NY, USA) supplemented with 10% FBS (Sigma-Aldrich, St. Louis, MO, USA). HEI-OC1 cells were incubated at 33 °C with 10% CO₂. Plasmid DNA transfection was performed using Lipofectamine 3000 transfection reagent (Life Technologies, Carlsbad, CA, USA). The mRFP-GFP tandem fluorescence-tagged LC3B (tfLC3B) was kindly provided by Dr. T. Yoshimori (Osaka University) [29], and the pcDNA3.1-Myc/His(-)A-*Uchl1* plasmid was kindly provided by Prof. K. J. Lee (Ewha Womans University, Korea).

[30]. For gene knockdown, small interfering RNA (siRNA) was transfected into HEI-OC1 cells using Lipofectamine RNAi Max reagent (Invitrogen, Carlsbad, CA, USA). The siRNAs were synthesized by Genolution Pharmaceuticals, Inc. (Seoul, South Korea). The target sequences of the siRNAs are 5'-GUUAGCCUAAAGUUUACUUCUU-3' and 5'-GAAGUAAAACUUUAGGGCUAACUU-3' for ubiquitin carboxyl-terminal hydrolase isozyme L1 (*Uchl1*), the nonspecific negative control (*siControl*). Cells transfected with plasmid DNA and siRNA were maintained for 24 h before GM treatment.

Primary SGC Culture

Dissociated SGCs were prepared as described previously [31]. In brief, the cochlea was dissected from SD rats on postnatal day 7. Lateral wall and organ of Corti tissues were removed, and SGCs were pooled and enzymatically digested with 0.25% trypsin/EDTA (Gendepot, Barker, TX USA) in phosphate-buffered saline (PBS) for 5 min at 37 °C. After centrifugation at 3000 rpm for 3 min to remove the supernatant, SGCs were plated on poly-D-lysine-coated coverslips (Superior-Marienfeld, Germany) in individual wells of 24-well culture plates and incubated in DMEM supplemented with 10% FBS (Gibco-BRL) and 0.06 mg/ml penicillin (Sigma-Aldrich, Steinheim, Germany) at 37 °C with 5% CO₂.

In Vivo GM Injection

Six-week-old male SD-rats were purchased from Daehan Bio Line (Chungbuk, South Korea). Eight rats were divided into two groups, normal saline-treated ($n = 4$) and GM-treated ($n = 4$) groups. GM at a dose of 220 mg/kg was administered intraperitoneally for five consecutive days. After day 10, all

rats were sacrificed, and the cochleae were harvested for histological evaluation. The Ajou University School of Medicine Institutional Animal Care and Use Committee approved the surgical procedures, which were performed in accordance with guidelines on the care and use of animals for experimental procedures.

Western Blot

Cells were lysed in radioimmunoprecipitation buffer (25 mM Tris HCl pH 8, 150 mM NaCl, 1% NP-40, 0.5% sodium deoxycholate, and 0.1% sodium dodecyl sulfate [SDS]) with a protease inhibitor cocktail (GenDEPOT). After extracting the proteins by centrifugation (13,000 rpm, 30 min), equal amounts of protein were loaded onto each lane of a gel, separated by SDS-polyacrylamide gel electrophoresis, and transferred onto a polyvinylidene difluoride (Millipore, Bedford, MA, USA) membrane using an electroblotting apparatus. Membranes were blocked for 1 h with 5% skim milk in PBS + 0.05% Tween 20. Subsequently, the membranes were probed with a primary antibody overnight at 4 °C. After that, the membranes were incubated with horseradish peroxidase conjugated secondary antibodies (1:5000, GenDEPOT, Katy, TX, USA) for 1 h at room temperature. Specific proteins were detected by Pierce ECL Western blotting substrate (Thermo Scientific, Pierce Biotechnology, Waltham, MA, USA). Proteins levels were quantified with densitometry analysis using ImageJ. The following primary antibodies were used: anti-UCHL1 (1:1000, Cell Signaling, Danvers, MA, USA; #13179), anti-microtubule-associated protein 1 light chain 3 (LC3) (1:2000, Sigma-Aldrich; L7543), anti-caspase 3 (1:1000, Cell Signaling; #9662), anti-SQSTM1/p62 (1:1000, Cell Signaling; #5114), anti-β-catenin (1:1000, Cell Signaling; #9562), anti-GAPDH (1:5000, Cell Signaling; #5174), and anti-β-actin (1:5000, Cell Signaling, #4970).

Immunofluorescence

Explants or cells were fixed in 4% paraformaldehyde (Biosesang, Gyeonggi-do, Korea) for 10 min at room temperature, washed, permeabilized, and blocked in PBS containing 0.2% Triton X-100 (1× PBST) and 1% bovine serum albumin in 1× PBST. Primary antibodies were dissolved in the same blocking solution at 4 °C overnight. The primary antibodies were anti-UCHL1 (1:500, Cell Signaling; #13179), anti-SOX2 (1:500, Cell Signaling; #4900), anti-TUJ1 (1:500, Cell Signaling; #5666), anti-myo7a (1:500, Proteus BioSciences, Proteus Biosciences Inc., Ramona, CA; 25-6700), and anti-lysosomal-associated membrane protein 1 (LAMP1) (1:200, Abcam, Cambridge, UK; ab24170). Samples were washed thoroughly and incubated with secondary antibodies tagged with fluorescein isothiocyanate (FITC) or cyanine 3 (Cy3) for 1 h at room temperature. F-actin was

stained with phalloidin-Texas Red (Invitrogen), and nuclei were counterstained with 4',6-diamidino-2-phenylindole (DAPI; Invitrogen). Coverslips were mounted onto slides with mounting medium (Vector Laboratories, Burlingame, CA, USA). The immunostained cells were observed using a Zeiss LSM 700 confocal microscope (Carl Zeiss Meditec, Jena, Germany).

Immunohistochemistry

Dissected cochleae were perfused with 4% paraformaldehyde and kept in the fixative overnight at 4 °C. They were washed with PBS, and decalcified with Calci-Clear Rapid (National Diagnostics, Atlanta, GA, USA) for 5 days. Following decalcification, cochleae were embedded in paraffin using a specialized automated tissue processing system. For paraffin-embedded tissues, cochleae were deparaffinized, rehydrated in graded alcohols, and processed for antigen retrieval using citrate buffer (pH 6.0) at 95 °C for 40 min. After cooling down, endogenous peroxidase was blocked in 3% H₂O₂ in methanol at room temperature for 10 min. Slides were incubated with 1% bovine serum albumin in PBST for 1 h. Primary antibodies and anti-UCHL1 (1:200, Cell Signaling; #13179) were applied overnight at 4 °C. Slides were washed and incubated with FITC-conjugated secondary antibody at room temperature for 1 h. The nuclei were counterstained with DAPI (1:10,000; Invitrogen). Images were taken with a Zeiss LSM 700 confocal microscope (Carl Zeiss Meditec).

Analysis of Cell Viability

HEI-OC1 cells were cultured into 96-well plates at a density of 3×10^3 cells/well for 24 h. After 24-h transfection of siRNA or plasmid DNA, cells were treated with GM for 48 h. Cell viability was determined using the water-soluble tetrazolium salt (WST-1) assay (Takara Bio, Shiga, Japan). At the end of the incubation, WST-1 solution was added to each well, and the cells were incubated for 4 h. Absorbance was measured using a microplate reader (Model 680; Bio-Rad, Hercules, CA, USA) at 450 nm. All assays were performed at least three times, and viability was normalized to the control.

Statistical Analysis

For the analysis of RNA-seq data, raw data were calculated as FPKM of each transcript in each sample by Cufflinks software. We excluded transcripts with more than one zeroed FPKM value for total samples. We added one to the FPKM value of the filtered transcript to facilitate log₂ transformation. Filtered data was transformed by the logarithm and normalized by the quantile normalization method. For each transcript, we conducted an independent *t* test between the case and control. We finally determined the significant result by

adjusting $|fold\ change| \geq 1.5$ and independent t test raw p value < 0.05 .

All values are expressed as the mean (\pm standard deviation). The statistical significance between the two groups was calculated by the Mann–Whitney U test and Kruskal–Wallis test for comparison of three groups using SPSS software version 12.0 (SPSS, Inc., Chicago, IL, USA). Probability values (P value) < 0.05 were considered statistically significant.

Results

Gene Expression Profiling During GM Treatment by RNA-Seq

Cochlear explants treated with 50 μ M GM showed a decrease in HC viability to $97.1 \pm 5.8\%$, $84.0 \pm 10.0\%$, and $44.2 \pm 19.8\%$ on days 1, 2, and 3, respectively, compared with day 0 ($100 \pm 0.0\%$) (Fig. 1a). To identify DEGs between the control and GM, RNA-seq analyses were performed on day 1 and 2 after GM treatment. The heat map of the hierarchical clustering method shows significant changes in levels of genes among three groups (Fig. 1b). There were 273 and 444 upregulated genes and 79 and 483 downregulated genes identified at day 1 and 2 post-GM treatment, respectively. There were 232 and 43 commonly up- and downregulated genes, respectively (Fig. 1c). The expression levels of known HC genes were also changed (Fig. S1). The results suggested the DEG patterns at day 1 and 2 post-GM treatment of cochleae were consistent with HC death in response to GM. GO analysis showed that genes related to the response of endogenous stimulus, vesicles, and the plasma membrane were preferentially up- or downregulated at day 1 post-GM treatment (Fig. 1d). At day 2 post-GM treatment, genes involved in the extracellular region, response to hormone stimulus, and vesicles were changed (Fig. 1e). In particular, genes related to vesicles were commonly affected at both day 1 and 2 post-GM treatment (Fig. 1f). The top ten genes associated with vesicles are listed in Table 1.

Protein Network Analysis of DEGs Indicated GM-Related Functional Modules

Most proteins do not operate alone but rather cooperate with other proteins to perform their functions. The study of PPI networks is not only important to predict the function of unidentified proteins from the evidence of already known PPIs but also to identify core candidate genes [32]. To identify the target genes putatively regulated by GM, we assessed the bioinformatics PPI for the common set of 275 significant genes at day 1 and 2 post-GM treatment (Fig. 1c). A total of 22 PPIs were constructed with the DEGs, and we selected the PPIs

based on the highest node value. This PPI network consisted of 280 nodes and 556 edges (Fig. 2a). We constructed a subnetwork with nodes that are in a first neighborhood (direct interaction) relationship with the DEGs. In the subnetwork, *Uchl1*, kinesin family member 5B (*Kif5b*), cyclin T1 (*Cnt1*), copine 3 (*Cpne3*), tankyrase (*Tnks*), and neural cell adhesion molecule 1 (*Ncam1*) were identified as the central genes (Fig. 2b). To validate our RNA-seq data, we performed qRT-PCR using new cochlear samples. A positive correlation between the RNA-seq analysis and qRT-PCR was observed as shown in Fig. 2c. This data indicates that our RNA-seq analysis was highly reliable.

Expression of the UCHL1 Protein in the Cochlea

UCHL1 is expressed predominantly in the brain and neuroendocrine system, and accounts for 1–2% of total brain soluble proteins [33]. Interestingly, cochlear tissue showed a predominant expression of UCHL1, as did brain tissue in both Western blot analyses with β -actin and GAPDH as relative controls (Fig. S2), and its expression was highest in SGCs, as expected (Fig. 3b). We further performed immunohistochemical staining of UCHL1 in adult rat cochlea. The double staining of antibodies against UCHL1 and TUJ1, a SGC specific marker, revealed that UCHL1 was predominantly expressed in SGCs, as well as efferent nerve terminal and nerve fibers connected to the HCs from the SGCs (Fig. 3a). To determine whether GM treatment could downregulate the levels of UCHL1, we compared UCHL1 expression differences between the GM-injected and non-injected SD-rats. The GM-injected rats showed downregulation of UCHL1 in both SGCs and efferent nerve terminals (Fig. 3c).

Knockdown or Inactivation of UCHL1 Accelerates GM-Induced Cell Death

UCHL1 has been reported to be upregulated in various tumor tissues and has been suggested to function as an oncogene in the progression of many cancers [34]. However, the results indicating whether UCHL1 facilitates cell death or survival in normal cells are controversial [35–37]. Therefore, we investigated whether reduced UCHL1 activity was able to affect GM-induced SGC death. For these experiments, we used the UCHL1 inhibitor, 3-amino-2-benzoyl-6-oxo-6,7-dihydrothieno[2,3-b]pyridine-5-carboxylic acid (LDN-91946), which is known to specifically inhibit UCHL1 activity [38]. After 50 μ M GM treatment for 48 h, the number of SGCs was decreased to $53 \pm 7\%$ compared with the control ($100 \pm 18\%$), and the decrease in SGCs was enhanced significantly by LDN-91946 treatment ($30 \pm 5\%$) (Fig. 4a, b).

Next, we observed the accumulation of LC3-II puncta in primary-cultured SGCs treated with GM compared to the control (treated with distilled water (DW)) by

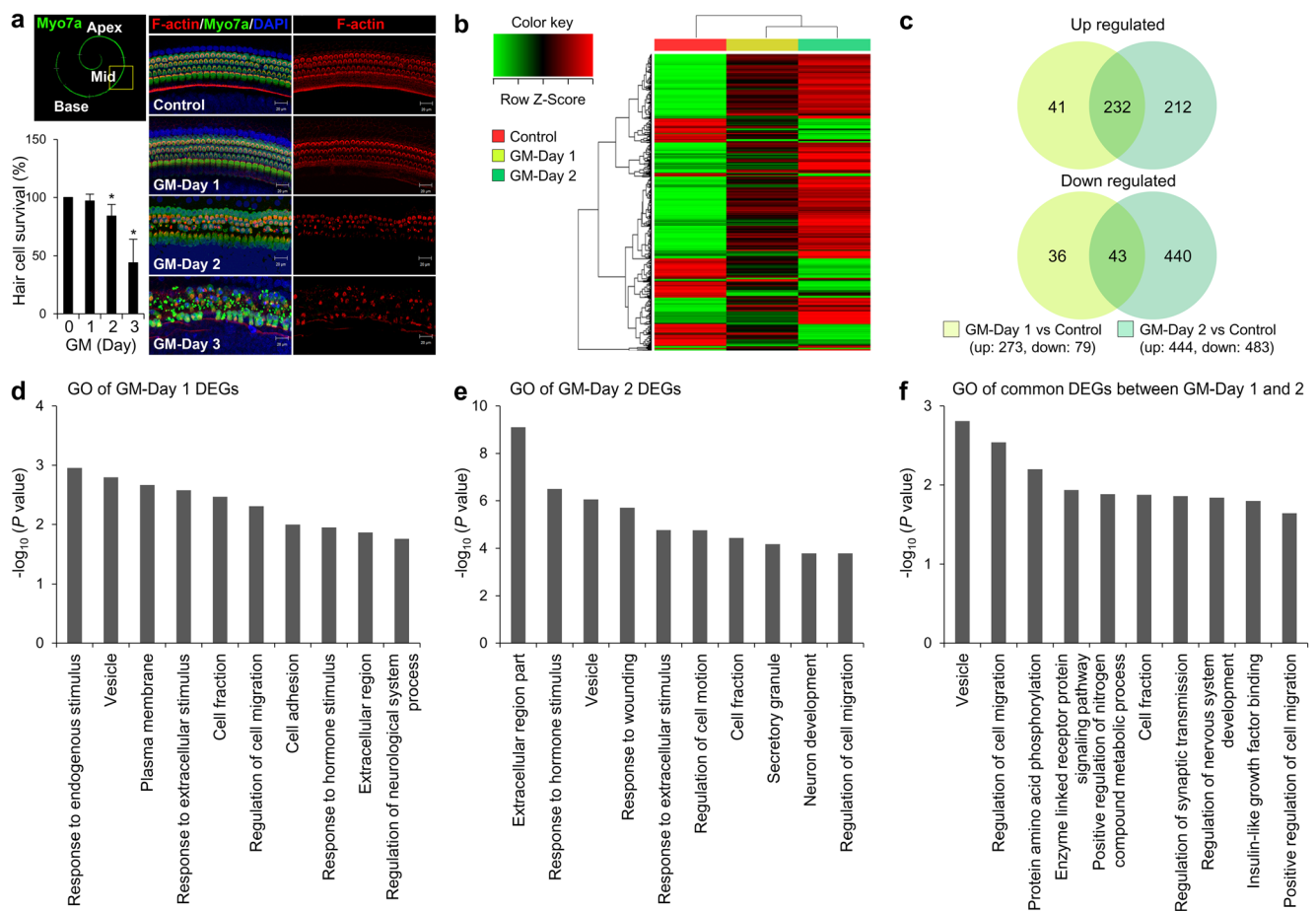


Fig. 1 Gene expression changes in the cochlea. **a** Confocal microscope images show the expression of myo7a and phalloidin in the middle turn of the organ of Corti treated with distilled water (DW) (control, $n = 3$) and gentamicin (GM, days 1, 2, and 3, $n = 3$, respectively). Histogram shows the mean viability of the hair cells. The data represent the mean \pm standard deviation of three independent organ of Corti samples (left panel) ($*P < 0.05$ vs day 0). **b** Heat maps of gene expression changes for control, day 1, and day 2 GM-treatment groups. **c** Venn diagrams summarizing

differentially expressed genes (DEGs) at day 1 (left circle) and day 2 (right circle) following GM treatment. The number in the area of overlap of the two circles indicates the number of genes whose expression changed at both time points. **d** Gene ontology (GO)-based functional enrichment analysis. GO terms significantly ($*P < 0.05$) enriched at day 1 (**e**), day 2 (**f**), and both time points (**g**). Log₁₀-transformed P values are shown on the Y -axis

immunofluorescence (Fig. 4c). However, unlike the immunofluorescence results, Western blot analysis did not show any change in LC3 lipidation, because primary SGCs did not proliferate and were highly differentiated, whereas other cells, including SCs and lateral wall fibrocytes, continuously proliferated (Fig. S3). Therefore, we used the auditory cell line HEI-OC1 in the following experiment. GM treatment temporarily increased the expression of UCHL1, which decreased in a time-dependent manner at 24 and 48 h, concomitant with an increase in LC3-II (Fig. 4d). *Uchl1* was down- or upregulated by siRNA, LDN-91946, or *Myc-Uchl1* overexpression plasmids to evaluate the effect of *Uchl1* on GM-induced cell death in HEI-OC1 cells. The transfection efficiency of siRNA and plasmid DNA was around 50 and 80%, respectively, as shown in supplementary Fig. S4. Cell viability was evaluated by WST-1 assay and counting of DAPI-positive cells. HEI-OC1 cells treated with *Uchl1* siRNA and LDN-91946 were

significantly accelerated cell death following GM treatment (Fig. 4e, f and S5a), compared to control siRNA-transfected or DMSO-treated cells, respectively. In contrast, cells overexpressing *Myc-Uchl1* exhibited increased cell viability compared to cells overexpressing *Myc* (Fig. 4g and S5b). We additionally investigated whether *Uchl1* decrease-induced cell death depends on autophagy. Double knockdown of *Uchl1* and autophagy-related 5 (*Atg5*) shows no additive effect on GM-induced cell death, compared to either *Uchl1* or *Atg5* knockdown alone (Fig. S6).

Knockdown of *Uchl1* Impaired Autophagosome Clearance and Stabilized Sequestosome 1 (SQSTM1/p62) and β -Catenin

UCHL1 is a member of the UCH deubiquitinating enzyme (DUB) family. Earlier studies showed that several DUB

Table 1 Top ten upregulated and downregulated vesicle-related genes at day 1 and 2 after GM

Gene	Description	Gene accession	Fold change	
			GM-Day 1	GM-Day 2
Upregulated				
<i>Ibsp</i>	Integrin-binding sialoprotein	NM_012587	5.19	5.75
<i>Bglap</i>	Bone gamma-carboxyglutamate (gla) protein	NM_013414	4.53	7.54
<i>Slc4a7</i>	Solute carrier family 4, sodium bicarbonate cotransporter, member 7	NM_058211	3.79	4.39
<i>Mib1</i>	Mindbomb E3 ubiquitin protein ligase 1	NM_001107405	3.56	3.72
<i>Lnpep</i>	Leucyl/cysteinyl aminopeptidase	NM_001113403	2.90	4.54
<i>Pdpk1</i>	3-Phosphoinositide dependent protein kinase-1	NM_031081	2.83	3.40
<i>Atp7a</i>	ATPase, Cu++ transporting, alpha polypeptide	NM_052803	2.71	4.07
<i>Kif1b</i>	Kinesin family member 1B	NM_057200	2.50	2.78
<i>Tmem33</i>	Transmembrane protein 33	NM_001034198	2.49	2.64
<i>Cd2ap</i>	CD2-associated protein	NM_181475	2.48	3.30
Downregulated				
<i>Scg3</i>	Secretogranin III	NM_053856	-1.64	-2.40
<i>Cfd</i>	Complement factor D (adipsin)	NM_001077642	-1.73	-2.36
<i>Vgf</i>	VGF nerve growth factor inducible	NM_030997	-1.76	-2.09
<i>Rab3b</i>	RAB3B, member RAS oncogene family	NM_031091	-1.82	-2.52
<i>Syt5</i>	Synaptotagmin V	NM_019350	-1.83	-2.98
<i>Thbs4</i>	Thrombospondin 4	NM_017133	-1.94	-2.93
<i>Iapp</i>	Islet amyloid polypeptide	NM_012586	-2.22	-2.15
<i>Sphk1</i>	Sphingosine kinase 1	NM_001270810	-2.24	-2.25
<i>Cspg5</i>	Chondroitin sulfate proteoglycan 5 (neuroglycan C)	NM_019284	-2.25	-2.00
<i>Gal</i>	Galanin/GMAP prepropeptide	NM_033237	-2.26	-4.21

family enzymes can regulate autophagy under normal growth or stress conditions [39]. Therefore, we investigated whether downregulation of *Uchl1* was able to affect GM-induced autophagy. The level of autophagy was monitored by the levels of LC3-II, an autophagosome marker. As shown in Fig. 5a, *Uchl1*-knockdown cells showed markedly increased LC3-II under both normal and GM conditions by Western blot. In contrast, *Uchl1*-overexpression decreases the LC3-II under GM condition (Fig. 5b). To illuminate whether the increase of autophagosomes was a result of increased formation or decreased fusion of autophagosomes with lysosomes, we performed tandem mRFP-GFP-tfLC3B construct fluorescence analysis. The RFP fluorescence is more stable in acidic compartments, whereas GFP fluorescence is rapidly quenched. Therefore, when autophagic flux is increased, the GFP/RFP ratio is decreased [27]. In the *siControl* cells, the GFP/RFP ratio was decreased, indicating that autophagic flux proceeds normally. In contrast, the GFP/RFP ratio was increased in *siUchl1*-knockdown cells, suggesting that the autophagosome is not efficiently degraded (Fig. 5c, e). We subsequently analyzed the effect of *Uchl1* overexpression on autophagic flux. As shown in Fig. 5d, f, the GFP/RFP ratio was considerably decreased in cells transfected with *Uchl1*, compared to *Myc*-transfected cells, in response GM. To evaluate inhibition of

autophagosome-lysosome fusion, we used LAMP1 as a lysosomal marker. As expected, LAMP1 did not co-localize with LC3 in the UCHL1-knockdown cells, regardless of GM treatment (Fig. S7). These results show that downregulation of *Uchl1* results in a blockade of the autophagic flux by impaired autophagosome clearance.

We next assessed the levels of SQSTM1/p62 in *Uchl1*-knockdown cells. p62, also known as SQSTM1, is an adaptor protein that brings polyubiquitinated proteins into nascent autophagosomes [40], and the disruption of autophagy results in the accumulation of SQSTM1/p62. Contradictory to the above results, siRNA knockdown of *Uchl1* decreased SQSTM1/p62 expression (Fig. 5a). Because the decreased expression of *Uchl1* might be associated with *SQSTM1/p62* transcriptional regulation, we measured *Sqstm1/p62* mRNA levels using qRT-PCR. However, *Uchl1* knockdown did not decrease *Sqstm1/p62* mRNA expression (Fig. 5g). Some DUB enzymes can act as regulators of protein stability by removing or editing ubiquitin chains that can be targets for proteasomal degradation [41]. Several studies have reported that UCHL1 plays a role in regulating protein stability. In particular, UCHL1 is required for stabilization of β -catenin through deubiquitination and upregulation of β -catenin/TCF transcriptional activity [36, 42, 43]. We also observed that *Uchl1*

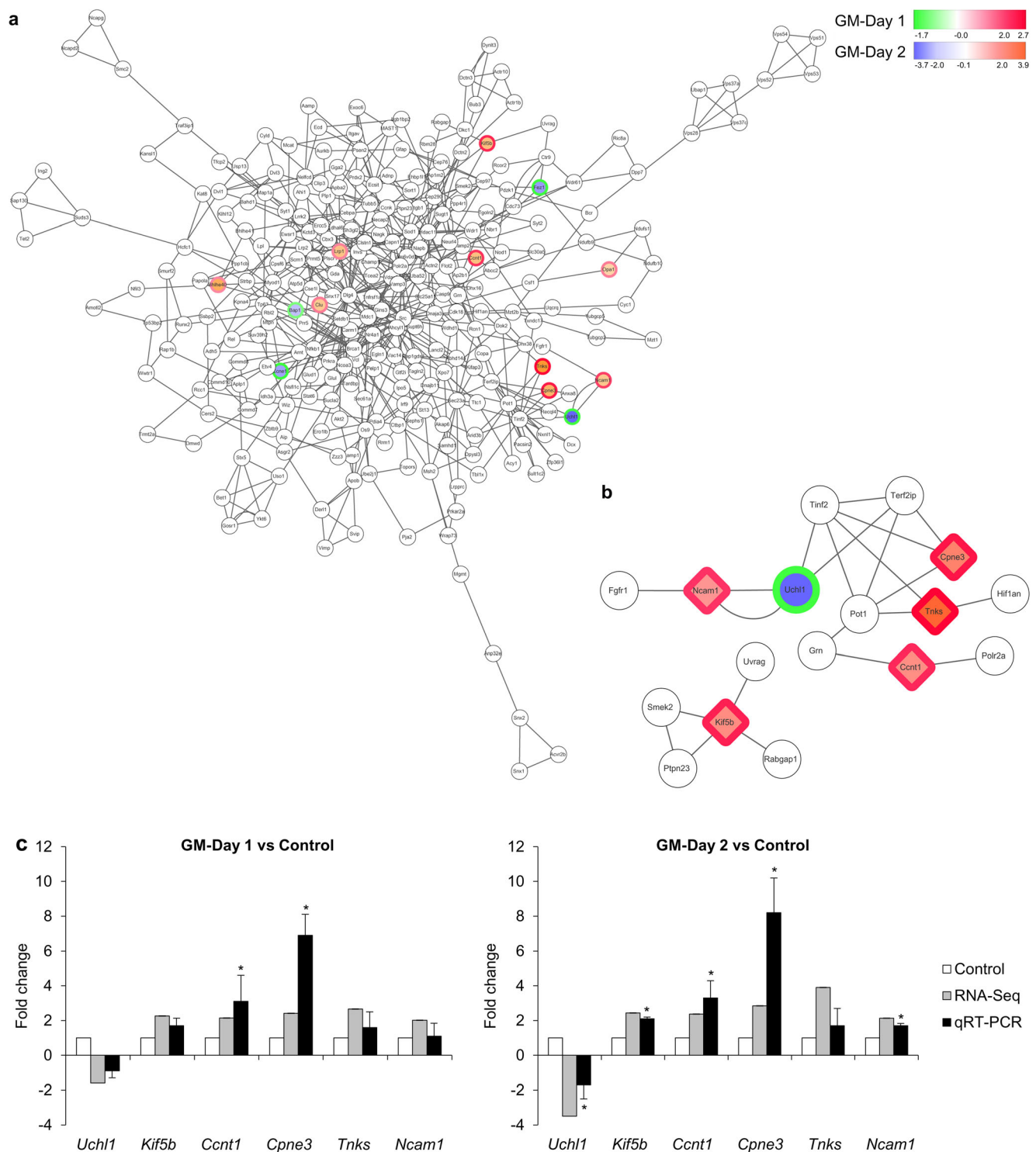


Fig. 2 Protein-protein interaction (PPI) network of the cochlear DEGs. **a** Overall PPI network of the DEGs. **b** Subnetwork clusters identified from the PPI network. Color scales are shown in the upper right. A new RNA sample was extracted from the cochlea at day 1 and day 2 (**c**) after gentamicin treatment. Validation of gene expression patterns from the RNA-

seq analysis (gray bar) by relative quantification through qRT-PCR (black bar). Relative expression levels of *Uch1*, *Kif5b*, *Ccnt1*, *Cpne3*, *Tnks*, and *Ncam1* are plotted on the Y-axis after normalization to control samples (white bar). Error bars represent standard deviation; $n = 3$, $*P < 0.05$ vs control

knockdown downregulated the expression of β -catenin in HEI-OC1 cells and upregulated caspase 3 activation against GM (Fig. 5a), whereas overexpression of *Uch1* shows β -

catenin upregulation and caspase 3 downregulation in response to GM (Fig. 5b). When *Uch1*-knockdown cells were treated for 4 h with the proteasome inhibitors MG132 and

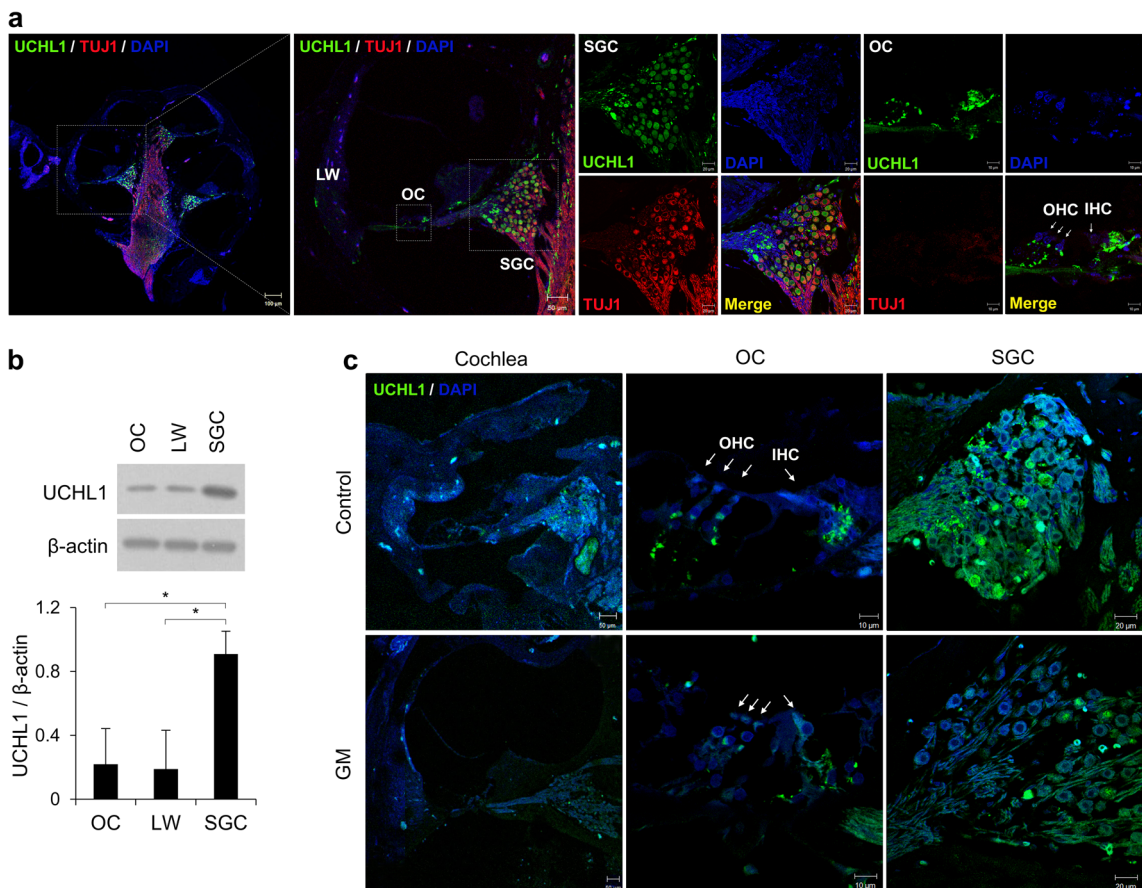


Fig. 3 Expression of UCHL1 in the rat cochlea. **a** Immunohistochemistry of SD-rat cochlea at 7 weeks. UCHL1 (green) is expressed in the SGCs, nerve fibers under IHCs, type I and II efferent and afferent nerve terminals, and LWS. The white square on merged images marks the magnified area. **b** Representative western blot of lysates from OC, LW, and SGC using anti-UCHL1. β -actin was used as the control for sample loading.

Error bars represent standard deviation; $n = 3$, $*P < 0.05$. c Immunohistochemistry of UCHL1 (green) in the middle turn of the cochlea injected with DW (control, upper panel) and gentamicin (lower panel). The white arrow indicates IHC and OHC. LW lateral wall, OC organ of Corti, OHC outer hair cell, IHC inner hair cell, SGC spiral ganglion cell

lactacystin, the reduced expression of SQSTM1/p62 and β -catenin, which was caused by *Uchl1* knockdown, was rescued (Fig. 5h and S8). A slight but insignificant increase of SQSTM1/p62 expression was observed following treatment with chloroquine (Fig. 5h). This result shows that *Uchl1* prevents proteasomal degradation of SQSTM1/p62 and β -catenin by using its deubiquitinating enzyme activity.

Discussion

A model of cochlear organotypic culture and next generation sequencing techniques are powerful tools to identify genes and pathways that contribute to the pathogenesis of GM-induced auditory cell death. The RNA-seq procedure showed that many genes were up- or downregulated in GM-treated organotypic cultures. Current RNA-seq data support our previous finding that GM treatment results in autophagosome accumulation due to impaired autophagy flux. GO analysis showed that 275 DEGs were involved in vesicles. Among

the top ten up- or downregulated DEGs, a kinesin-like protein, *Kif1b*, was previously reported to be co-localized with lysosomal markers and involved in lysosome transport. Moreover, the knockdown of *Kif1b* impaired the nutrient-controlled activation of mTORC1, a regulator of autophagy [44]. Upregulation of *Kif1b* was verified in the cochlea after noise trauma [45]. Transmembrane protein 33 (*Tmem33*) has been reported to be a novel regulator of the endoplasmic reticulum stress-induced unfolded protein response signaling cascade in cancer cells [46]. Ras-related protein, *Rab3b*, which is highly expressed in the vesicle fraction [47], mediates endocytosis and biosynthetic protein transport [48]. Significant decreases of *Rab3b* mRNA levels following cisplatin treatment were observed in rat organotypic culture [49]. These genes may be involved in the GM-induced appearance of vesicles and enlargement of lysosomes.

Of the six putative genes in the PPI subnetwork, *Ncam1* and *Uchl1* have been reported to be expressed in the cochlea. The neural cell adhesion molecule, *Ncam*, is expressed along the growth path of the nerve fibers for synaptogenesis and

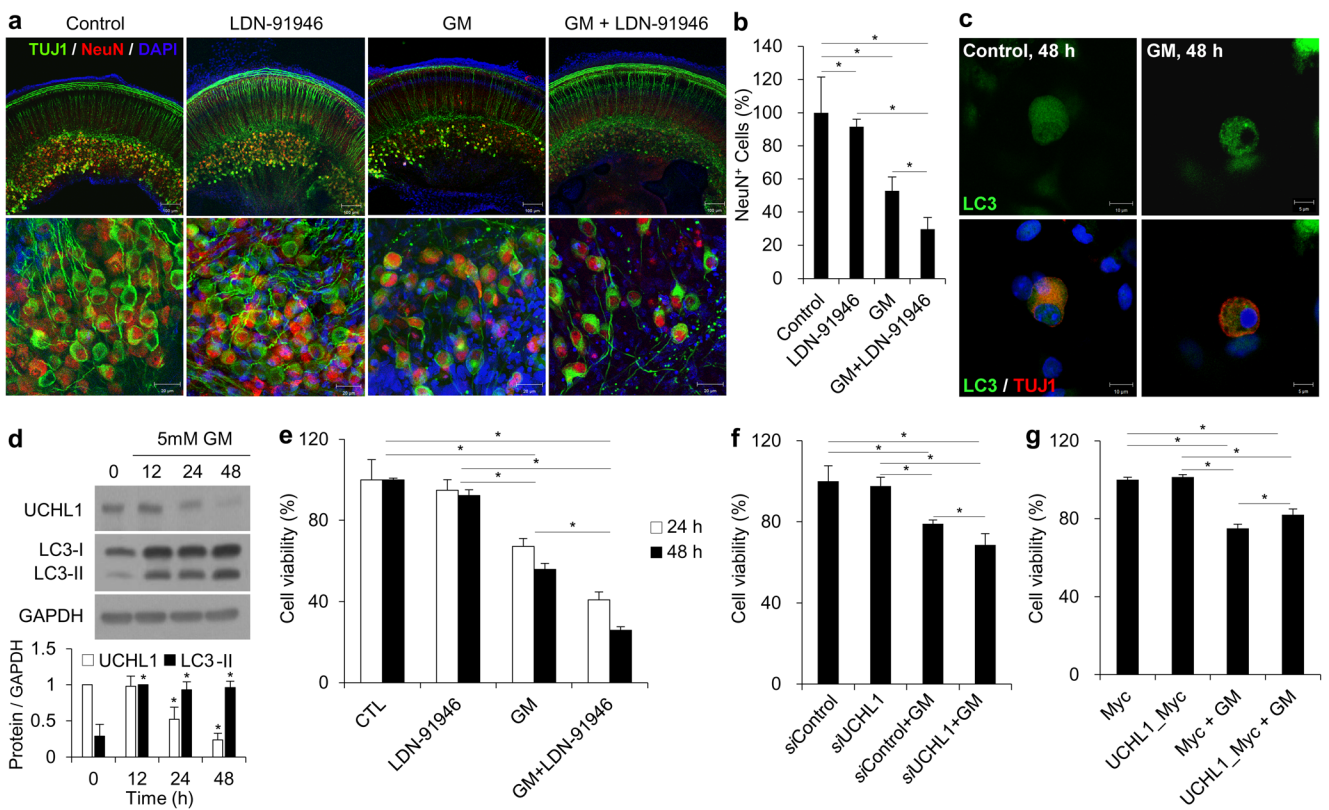


Fig. 4 Downregulation of UCHL1 enhanced gentamicin (GM)-induced auditory cell death. **a** Organotypic cultures from the middle cochleae 48 h after DW, 50 μ M GM, 10 μ M LDN-91946, and 50 μ M GM + 10 μ M LDN-91946 treatment. LDN-91946 was pre-treated for 4 h and co-treated with GM. The spiral ganglion cells (SGCs) were stained with a TUJ1 (green) and NeuN (red) antibody. **b** The graph shows the quantitative results of the cochlear SGC counts. Data represent the mean \pm standard deviation ($n = 3$) (* $P < 0.05$). **c** Representative confocal images confirmed TUJ1 (red) and LC3 (green)-expressing SGCs treated with DW (control) and 50 μ M GM for 48 h. **d** Time-dependent change of UCHL1 expression from HEI-OC1 cells treated with 5 mM GM. Western blot data was quantified and normalized to GAPDH. Data represent the mean \pm

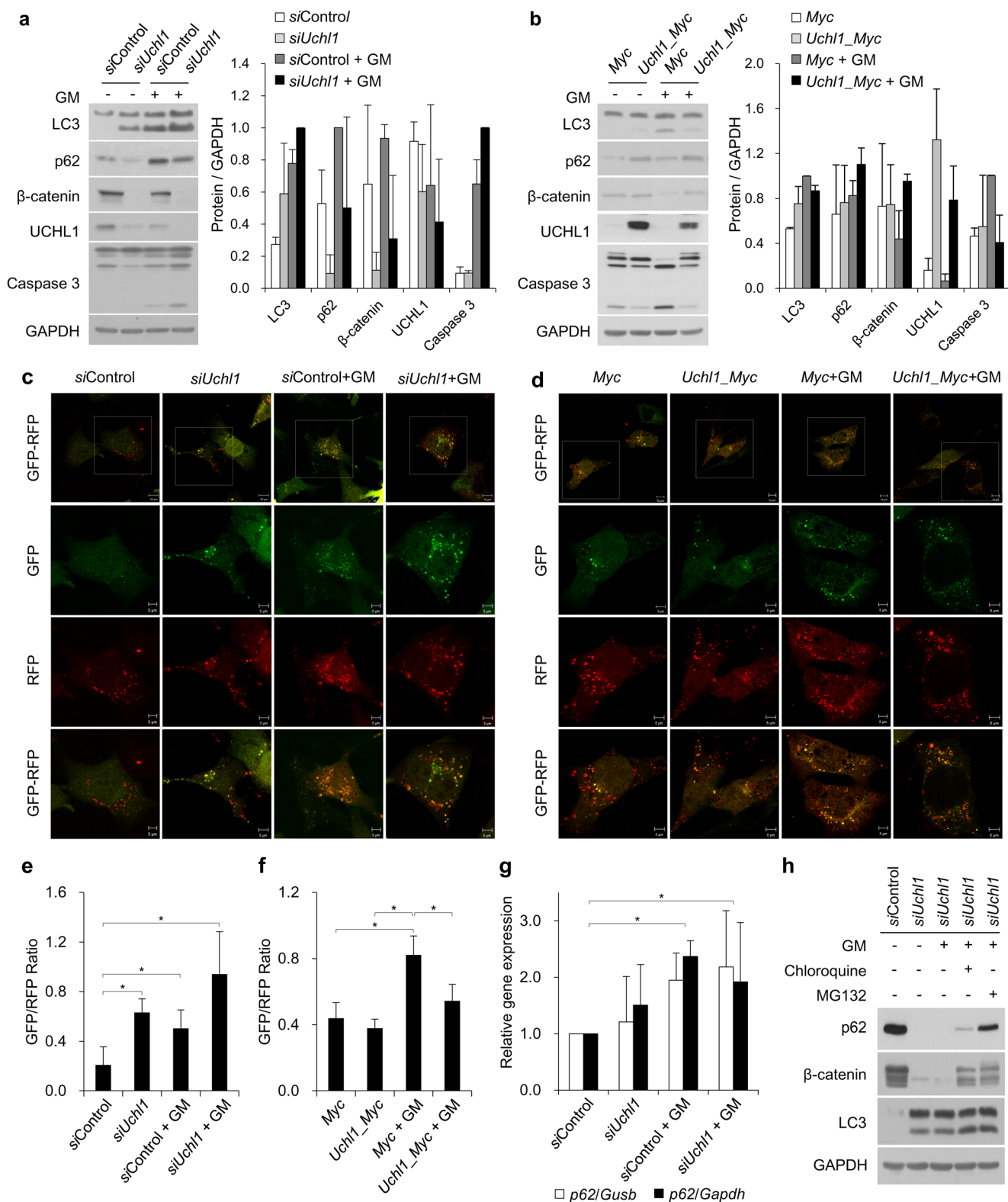
standard deviation ($n = 3$) (* $P < 0.05$ vs day 0). **e** HEI-OC1 cells were treated with the UCHL1 inhibitor, LDN-91946 (10 μ M), during exposure to 5 mM GM for 24 and 48 h. **f** Cells were transfected with control small interfering RNA (siRNA) or *Uchl1* siRNA for 24 h and subsequently treated with or without 5 mM GM for 48 h. **g** Cells were transfected with *Myc* or *Uchl1-Myc* for 24 h and were subsequently treated with or without 5 mM GM for 48 h. Cell viability was quantified using water-soluble tetrazolium salt (WST-1) assays. The relative percent cell viability was calculated by comparing samples with the viability of control HEI-OC1 cells. The bar graph is presented as mean \pm standard deviation ($n = 3$). Statistical analyses were performed using Mann–Whitney *U* tests (* $P < 0.05$)

axon guidance in the organ of Corti [50]. Furthermore, using Lunatic Fringe (*Lfng*)-GFP transgenic mice, recent studies showed that *Uchl1* was expressed in a subpopulation of non-sensory supporting cells (SCs), and it may contribute to HC or neuron differentiation [51]. The UCHL1 protein was, however, also detectable in vestibular HCs [52]. In our study, *Uchl1* was downregulated by GM in a time-dependent manner, and deficiency of *Uchl1* was found to be associated with the autophagy/lysosomal pathway upon damage or pathological condition [39, 53].

UCHL1 is a deubiquitinating enzyme that cleaves ubiquitin from polyubiquitin chains at its carboxyl terminal, and stabilizes monoubiquitin. Thus, UCHL1 may play an important role in maintaining the free ubiquitin pool for the UPS [54]. UCHL1 is expressed predominantly in the brain and neuroendocrine system with functional roles in maintenance of synaptic structures, ubiquitin stabilization and turnover, and regulation of proteasomal and lysosomal degradation [54].

Dysfunction of UCHL1 has been reported in many neurodegenerative diseases, including Alzheimer’s and Parkinson’s diseases [55]. In addition to neurodegenerative disease, recent

Fig. 5 UCHL1 is required for autophagosome clearance. Western blot analysis of *Uchl1* knockdown (a) and overexpression (b) with or without 5 mM gentamicin (GM) for 48 h in HEI-OC1 cells. GAPDH levels were determined as a loading control. **c, d** HEI-OC1 cells were co-transfected with *siControl*, *siUchl1*, *Myc*, *Uchl1_Myc*, and *tFLC3* plasmids. After 24 h, the cells were treated with GM for 48 h, fixed, and analyzed by microscopy. The white square on merged images marks the magnified area. **e, f** Statistical analysis of GFP/RFP ratio. Values were represented as mean \pm standard deviation ($n = 3$). **g** Quantitative RT-PCR of *p62* mRNA level in *siControl* and *siUchl1* knockdown cells. *Gapdh* and *Gusb* were used as an internal control. Data represent the mean \pm standard deviation ($n = 3$). Statistical analyses were performed using Mann–Whitney *U* tests (* $P < 0.05$). **f** UCHL1 knockdown cells were treated with GM. After treatment with GM for 48 h, cells were treated with chloroquine (CQ, 50 μ M) and MG132 (5 μ M) for 4 h. GAPDH levels were determined as a loading control



reports suggest that UCHL1 plays a role in physiological and pathological processes including development, aging, carcinogenesis, and cell death [56]. The functional significance of the UCHL1 gene in hearing problems is currently not well

known, but a recent study reported that UCHL1 may play an important role in maintaining the level of monoubiquitin to promote proteolysis by initiating the UPS system to protect the auditory cortex from oxidative stress during aging [57].

In the present study, *Uchl1* was found to be downregulated following GM treatment. *Uchl1* inhibition by siRNA and the pharmacological inhibitor, LDN-91946, in both cochlear explants and HEI-OC1 cells led to exacerbated GM-induced auditory cell death. A recent study also indicated a significant decrease of UCHL1 protein in the subventricular zone with age-dependent neurodegenerative diseases [58]. The significant role of UCHL1 has also been reported to be associated with several human diseases, including type 2 diabetes [53, 59], epilepsy [60], nephropathy [61], and several malignancies [62, 63]. Decreased UCHL1 can be harmful in normal cells, but beneficial in cancer cells by potentiating sensitivity in cancer cells against anti-cancer drugs. Some studies have reported on the mechanistic links between UCHL1 and the UPS, cell cycle, protein stabilization, and autophagy.

Our previous study reported that autophagic flux participates in delayed GM-induced ototoxicity [11], and rapamycin attenuates GM-induced auditory cell death by stimulating autophagy. Autophagy is normally able to regulate intracellular protein turnover to maintain cellular homeostasis. However, when autophagy is compromised, by GM for example, it can be implicated in the pathogenesis. Interestingly, Reynolds JP et al. reported that rapamycin can attenuate processes associated with epileptogenesis, including hippocampal cell death and axonal sprouting through mammalian target of rapamycin (mTOR) signaling-mediated upregulation of UCHL1 [60]. Recently, Yan C et al. did a genome-wide screen of 55 human DUBs and found out that a certain number of the human DUBs affected autophagy in diverse aspects. One of them, UCHL1 interacts with LC3 and inhibits autophagosome formation depending on its DUB activity [64]. In addition, recent reports have shown that defective *Uchl1* exacerbates the autophagy/lysosomal degradation disruption caused by high expression of human islet amyloid polypeptide [53]. In this study, we also found that silencing of the *Uchl1* protein blocked autophagic flux using mRFP-GFP-tfLC3B and co-localization of LAMP1 and LC3. This suggests that GM-induced downregulation of UCHL1 might negatively regulate the autophagosome and lysosome fusion step in response to GM treatment.

The expression of SQSTM1/p62 in the regulation of GM-induced impairment of autophagic flux has been controversial. SQSTM1/p62 is a multifunctional adaptor protein that possesses an ubiquitin-binding domain and LC3-interacting region and is therefore able to interact with ubiquitinated cargo in the core autophagic machinery [40]. Since SQSTM1/p62 is degraded by autophagy, decreased levels of SQSTM1/p62 may be used as an autophagic flux marker. However, in the present study, the decreased expression of SQSTM1/p62 in cells with *Uchl1* siRNA was not accompanied by changes in acridine orange, indicating an acidic vacuole in cells, including lysosomes and autolysosomes. Acridine orange is a nucleic acid, a lysosomotropic metachromatic green

fluorophore that accumulates in an acidic compartment, shifting its emission to longer wavelengths (650 nm, red fluorescence). It showed the accumulation of LC3 and an increase in the ratio of GFP/RFP, indicating impairment of autophagic flux (Fig. 5). Therefore, two possible hypotheses can be considered. First, HEI-OC1 cells treated with *Uchl1* siRNA may affect the autophagic flux via a SQSTM1/p62-independent pathway (e.g., NBR1 and NDP52). Second, disruption of SQSTM1/p62 protein stabilization by knockdown of *Uchl1* can impair autophagic flux. In this context, β-catenin [36, 42, 43], p53 [65], and HIF-1α [66] have been suggested. Further study is needed to understand the differential results of SQSTM1/p62 on the impairment of autophagic flux.

The doses used are important in toxic mechanistic studies, because the cell-death pathway (necrosis, apoptosis, or autophagy) can differ according to the dose. In the present study, the concentrations of gentamicin that reduced cell viability by 15–25% at 48 h and increased the expression of the autophagosome marker LC3 were determined. The appropriate concentrations of gentamicin were 50 μM in organotypic culture and 5 mM in HEI-OC1 cells. The concentration of gentamicin that is toxic is typically higher in cell lines cultured *in vitro* than that *in vivo* because of the different environmental conditions.

An adult cochlea expresses UCHL1 in SGCs, nerve fibers under inner hair cells, and type I and II efferent and afferent nerve terminals as shown in Fig. 3. Another important role for UCHL1 is the maintenance of neuronal health and synaptic stability and integrity by providing a sufficient level of mono-ubiquitin [67]. From the PPI network results, we observed an interconnection between *Uchl1* and *Ncam*. *Ncam* has been reported to be important for SGC survival and neurite growth in the organ of Corti [68]. Furthermore, recent studies in the human fetal brain have also shown that *Uchl1* is a novel interaction partner of *Ncam* through the de-ubiquitination and recycling of *Ncam* for normal functions in the nervous system [52]. Therefore, we cannot rule out the possibility that the inhibition of *Uchl1* has some direct effect on SGCs. *Uchl1* may be partly involved in the synaptic dysfunction between HCs and SGCs.

In summary, downregulation of the *UCHL1* gene is involved in GM-induced ototoxicity. Further, our data indicate that the dysregulation of *Uchl1* is deleterious to auditory cell survival through impaired autophagic flux. This is the first report to demonstrate the role of UCHL1 in GM-induced autophagic cell death, and we suggest that the involvement of UCHL1 in drug-induced ototoxicity may be worth exploring.

Acknowledgments This research was supported by the Basic Science Research Program through the National Research Foundation of Korea (NRF) funded by the Ministry of Education, Science, and Technology (NRF-2019R1A2C2002384).

Compliance with Ethical Standards

Conflict of Interest The authors declare that they have no conflict of interest.

References

- Ryan A, McGee TJ (1977) Development of hearing loss in kanamycin treated chinchillas. *Ann Otol Rhinol Laryngol* 86(2 pt. 1): 176–182. <https://doi.org/10.1177/000348947708600207>
- Kaloyanides GJ, Pastoriza-Munoz E (1980) Aminoglycoside nephrotoxicity. *Kidney Int* 18(5):571–582. <https://doi.org/10.1038/ki.1980.175>
- Mulheran M, Degg C, Burr S, Morgan DW, Stableforth DE (2001) Occurrence and risk of cochleotoxicity in cystic fibrosis patients receiving repeated high-dose aminoglycoside therapy. *Antimicrob Agents Chemother* 45(9):2502–2509. <https://doi.org/10.1128/AAC.45.9.2502-2509.2001>
- Hashino E, Sher M, Salvi RJ (1997) Lysosomal targeting and accumulation of aminoglycoside antibiotics in sensory hair cells. *Brain Res* 777(1–2):75–85. [https://doi.org/10.1016/S0006-8993\(97\)00977-3](https://doi.org/10.1016/S0006-8993(97)00977-3)
- Hashino E, Sher M (1995) Endocytosis of aminoglycoside antibiotics in sensory hair cells. *Brain Res* 704(1):135–140. [https://doi.org/10.1016/0006-8993\(95\)01198-6](https://doi.org/10.1016/0006-8993(95)01198-6)
- Huth ME, Ricci AJ, Cheng AG (2011) Mechanisms of aminoglycoside ototoxicity and targets of hair cell protection. *Int J Otolaryngol* 2011:937861. <https://doi.org/10.1155/2011/937861>
- Wang Q, Kachelmeier A, Steyger PS (2010) Competitive antagonism of fluorescent gentamicin uptake in the cochlea. *Hear Res* 268(1–2):250–259. <https://doi.org/10.1016/j.heares.2010.06.008>
- Sha SH, Schacht J (1999) Formation of reactive oxygen species following bioactivation of gentamicin. *Free Radic Biol Med* Feb 26(3–4):341–347. [https://doi.org/10.1016/S0891-5849\(98\)00207-X](https://doi.org/10.1016/S0891-5849(98)00207-X)
- Darrouzet J, Guilhaume A (1974) Ototoxicity of kanamycin studied day by day. Experimental electron microscopic study. *Rev Laryngol Otol Rhinol (Bord)* 95(9–10):601–621
- Hirose K, Westrum LE, Cunningham DE et al (2004) Electron microscopy of degenerative changes in the chick basilar papilla after gentamicin exposure. *J Comp Neurol* 470(2):164–180. <https://doi.org/10.1002/cne.11046>
- Kim YJ, Tian C, Kim J, Shin B, Choo OS, Kim YS, Choung YH (2017) Autophagic flux, a possible mechanism for delayed gentamicin-induced ototoxicity. *Sci Rep* 01(7):41356. <https://doi.org/10.1038/srep41356>
- Roehm P, Hoffer M, Balaban CD (2007) Gentamicin uptake in the chinchilla inner ear. *Hear Res* 230(1–2):43–52. <https://doi.org/10.1016/j.heares.2007.04.005>
- Oishi N, Duscha S, Boukari H, Meyer M, Xie J, Wei G, Schrepfer T, Roschitzki B et al (2015) XBP1 mitigates aminoglycoside-induced endoplasmic reticulum stress and neuronal cell death. *Cell Death Dis* 14(6):e1763. <https://doi.org/10.1038/cddis.2015.108>
- Kim BY, Bae WY, Hur DY, Kim JR, Koh TK, Lee TH, Park GB (2016) Effects of Memantine on aminoglycoside-induced apoptosis of spiral ganglion cells in guinea pigs. *Otolaryngol Head Neck Surg* 155(1):147–154. <https://doi.org/10.1177/0194599816639297>
- Trapnell C, Pachter L, Salzberg SL (2009) TopHat: discovering splice junctions with RNA-Seq. *Bioinformatics* 25(9):1105–1111. <https://doi.org/10.1093/bioinformatics/btp120>
- Trapnell C, Williams BA, Pertea G, Mortazavi A, Kwan G, van Baren MJ, Salzberg SL, Wold BJ et al (2010) Transcript assembly and quantification by RNA-Seq reveals unannotated transcripts and isoform switching during cell differentiation. *Nat Biotechnol* 28(5): 511–515. <https://doi.org/10.1038/nbt.1621>
- Huang d W, Sherman BT, Lempicki RA (2009) Systematic and integrative analysis of large gene lists using DAVID bioinformatics resources. *Nat Protoc* 4(1):44–57. <https://doi.org/10.1038/nprot.2008.211>
- Keshava Prasad TS, Goel R, Kandasamy K, Keerthikumar S, Kumar S, Mathivanan S, Telikicherla D, Raju R et al (2009) Human protein reference database—2009 update. *Nucleic Acids Res* 37(Database issue):D767–D772. <https://doi.org/10.1093/nar/gkn892>
- Chatr-Aryamontri A, Breitkreutz BJ, Heinicke S et al (2013) The BioGRID interaction database: 2013 update. *Nucleic Acids Res* 41(Database issue):D816–D823. <https://doi.org/10.1093/nar/gks1158>
- Kerrien S, Aranda B, Breuza L, Bridge A, Broackes-Carter F, Chen C, Duesbury M, Dumousseau M et al (2012) The IntAct molecular interaction database in 2012. *Nucleic Acids Res* 40(Database issue):D841–D846. <https://doi.org/10.1093/nar/gkr1088>
- Licata L, Brigandt L, Peluso D, Perfetto L, Iannuccelli M, Galeota E, Sacco F, Palma A et al (2012) MINT, the molecular interaction database: 2012 update. *Nucleic Acids Res* 40(Database issue):D857–D861. <https://doi.org/10.1093/nar/gkr930>
- Chelliah V, Laibe C, Le Novere N (2013) BioModels database: a repository of mathematical models of biological processes. *Methods Mol Biol* 1021:189–199. https://doi.org/10.1007/978-1-62703-450-0_10
- Turner B, Razick S, Turinsky AL, Vlasblom J, Crowdny EK, Cho E, Morrison K, Donaldson IM et al (2010) iRefWeb: Interactive analysis of consolidated protein interaction data and their supporting evidence. *Database (Oxford)* 12(2010):baq023. <https://doi.org/10.1093/database/baq023>
- Lee K, Byun K, Hong W, Chuang HY, Pack CG, Bayarsaikhan E, Paek SH, Kim H et al (2013) Proteome-wide discovery of mislocated proteins in cancer. *Genome Res* 23(8):1283–1294. <https://doi.org/10.1101/gr.155499.113>
- Lopes CT, Franz M, Kazi F et al (2010) Cytoscape Web: an interactive web-based network browser. *Bioinformatics* 26(18):2347–2348. <https://doi.org/10.1093/bioinformatics/btq430>
- Bader GD, Hogue CW (2003) An automated method for finding molecular complexes in large protein interaction networks. *BMC Bioinformatics* 13(4):2. <https://doi.org/10.1186/1471-2105-4-2>
- Nagy I, Caelers A, Monge A, Bonabi S, Huber AM, Bodmer D (2007) NF-κappaB-dependent apoptotic hair cell death in the auditory system. *Audiol Neurotol* 12(4):209–220. <https://doi.org/10.1159/000101328>
- Chen J, Chu H, Xiong H, Chen Q, Zhou L, Bing D, Liu Y, Gao Y et al (2012) Expression patterns of Ca(V)1.3 channels in the rat cochlea. *Acta Biochim Biophys Sin Shanghai* 44(6):513–518. <https://doi.org/10.1093/abbs/gms024>
- Kimura S, Noda T, Yoshimori T (2007) Dissection of the autophagosome maturation process by a novel reporter protein, tandem fluorescent-tagged LC3. *Autophagy* 3(5):452–460. <https://doi.org/10.4161/auto.4451>
- Song IK, Kim HJ, Magesh V, Lee KJ (2018) Ubiquitin C-terminal hydrolase-L1 plays a key role in angiogenesis by regulating hydrogen peroxide generated by NADPH oxidase 4. *Biochem Biophys Res Commun* 495(1):1567–1572. <https://doi.org/10.1016/j.bbrc.2017.11.051>
- Zheng JL, Stewart RR, Gao WQ (1995) Neurotrophin-4/5 enhances survival of cultured spiral ganglion neurons and protects them from cisplatin neurotoxicity. *J Neurosci* 15(7 Pt 2):5079–5087. <https://doi.org/10.1523/JNEUROSCI.15-07-05079.1995>

32. Rao VS, Srinivas K, Sujini GN, Kumar GNS (2014) Protein-protein interaction detection: methods and analysis. *Int J Proteomics* 2014:147648. <https://doi.org/10.1155/2014/147648>
33. Doran JF, Jackson P, Kynoch PA et al (1983) Isolation of PGP 9.5, a new human neurone-specific protein detected by high-resolution two-dimensional electrophoresis. *J Neurochem* 40(6):1542–1547. <https://doi.org/10.1111/j.1471-4159.1983.tb08124.x>
34. Hurst-Kennedy J, Chin LS, Li L (2012) Ubiquitin C-terminal hydrolase l1 in tumorigenesis. *Biochem Res Int* 2012:123706. <https://doi.org/10.1155/2012/123706>
35. Kabuta T, Mitsui T, Takahashi M et al (2013) Ubiquitin C-terminal hydrolase L1 (UCH-L1) acts as a novel potentiator of cyclin-dependent kinases to enhance cell proliferation independently of its hydrolase activity. *J Biol Chem* 288(18):12615–12626. <https://doi.org/10.1074/jbc.M112.435701>
36. Zhong J, Zhao M, Ma Y et al (2012) UCHL1 acts as a colorectal cancer oncogene via activation of the beta-catenin/TCF pathway through its deubiquitinating activity. *Int J Mol Med* 30(2):430–436. <https://doi.org/10.3892/ijmm.2012.1012>
37. Shen H, Sikorska M, Leblanc J et al (2006) Oxidative stress regulated expression of ubiquitin carboxyl-terminal hydrolase-L1: role in cell survival. *Apoptosis* 11(6):1049–1059. <https://doi.org/10.1007/s10495-006-6303-8>
38. Mermier AH, Case A, Stein RL et al (2007) Structure-activity relationship, kinetic mechanism, and selectivity for a new class of ubiquitin C-terminal hydrolase-L1 (UCH-L1) inhibitors. *Bioorg Med Chem Lett* 17(13):3729–3732. <https://doi.org/10.1016/j.bmcl.2007.04.027>
39. Magraoui FE, Reidick C, Meyer HE, Platta H (2015) Autophagy-related deubiquitinating enzymes involved in health and disease. *Cells* 4(4):596–621. <https://doi.org/10.3390/cells4040596>
40. Pankiv S, Clausen TH, Lamark T et al (2007) p62/SQSTM1 binds directly to Atg8/LC3 to facilitate degradation of ubiquitinated protein aggregates by autophagy. *J Biol Chem* 282(33):24131–24145. <https://doi.org/10.1074/jbc.M702824200>
41. Komander D, Clague MJ, Urbe S (2009) Breaking the chains: structure and function of the deubiquitinases. *Nat Rev Mol Cell Biol* 10(8):550–563. <https://doi.org/10.1038/nrm2731>
42. Bheda A, Yue W, Gullapalli A, Whitehurst C, Liu R, Pagano JS, Shackelford J (2009) Positive reciprocal regulation of ubiquitin C-terminal hydrolase L1 and beta-catenin/TCF signaling. *PLoS One* 4(6):e5955. <https://doi.org/10.1371/journal.pone.0005955>
43. Taya S, Yamamoto T, Kanai-Azuma M, Wood SA, Kaibuchi K (1999) The deubiquitinating enzyme fam interacts with and stabilizes beta-catenin. *Genes Cells* 4(12):757–767. <https://doi.org/10.1046/j.1365-2443.1999.00297.x>
44. Pous C, Codogno P (2011) Lysosome positioning coordinates mTORC1 activity and autophagy. *Nat Cell Biol* 13(4):342–334. <https://doi.org/10.1038/ncb0411-342>
45. Gong TW, Hegeman AD, Shin JJ et al (1996) Identification of genes expressed after noise exposure in the chick basilar papilla. *Hear Res* 96(1–2):20–32. [https://doi.org/10.1016/0378-5955\(96\)00013-5](https://doi.org/10.1016/0378-5955(96)00013-5)
46. Sakabe I, Hu R, Jin L, Clarke R, Kasid UN (2015) TMEM33: a new stress-inducible endoplasmic reticulum transmembrane protein and modulator of the unfolded protein response signaling. *Breast Cancer Res Treat* 153(2):285–297. <https://doi.org/10.1007/s10549-015-3536-7>
47. Pavlos NJ, Gronborg M, Riedel D et al (2010) Quantitative analysis of synaptic vesicle Rabs uncovers distinct yet overlapping roles for Rab3a and Rab27b in Ca²⁺-triggered exocytosis. *J Neurosci* 30(40):13441–13453. <https://doi.org/10.1523/JNEUROSCI.0907-10.2010>
48. Binotti B, Pavlos NJ, Riedel D, Wenzel D, Vorbrüggen G, Schalk AM, Kühnel K, Boyken J et al (2015) The GTPase Rab26 links synaptic vesicles to the autophagy pathway. *Elife* 02(4):e05597. <https://doi.org/10.7554/elife.05597>
49. Wang P, Zhang P, Huang J, Li M, Chen X (2013) Trichostatin A protects against cisplatin-induced ototoxicity by regulating expression of genes related to apoptosis and synaptic function. *Neurotoxicology* 37:51–62. <https://doi.org/10.1016/j.neuro.2013.03.007>
50. Whitton DS, Rutishauser US (1990) NCAM in the organ of Corti of the developing mouse. *J Neurocytol* 19(6):970–977. <https://doi.org/10.1007/BF01186824>
51. Maass JC, Gu R, Cai T, Wan YW, Cantellano SC, Asprer JST, Zhang H, Jen HI et al (2016) Transcriptomic analysis of mouse cochlear supporting cell maturation reveals large-scale changes in notch responsiveness prior to the onset of hearing. *PLoS One* 11(12):e0167286. <https://doi.org/10.1371/journal.pone.0167286>
52. Herget M, Scheibinger M, Guo Z, Jan TA, Adams CM, Cheng AG, Heller S (2013) A simple method for purification of vestibular hair cells and non-sensory cells, and application for proteomic analysis. *PLoS One* 8(6):e66026. <https://doi.org/10.1371/journal.pone.0066026>
53. Costes S, Gurlo T, Rivera JF, Butler PC (2014) UCHL1 deficiency exacerbates human islet amyloid polypeptide toxicity in beta-cells: Evidence of interplay between the ubiquitin/proteasome system and autophagy. *Autophagy* 10(6):1004–1014. <https://doi.org/10.4161/auto.28478>
54. Ristic G, Tsou WL, Todi SV (2014) An optimal ubiquitin-proteasome pathway in the nervous system: the role of deubiquitinating enzymes. *Front Mol Neurosci* 7:72. <https://doi.org/10.3389/fnmol.2014.00072>
55. Bilguvar K, Tyagi NK, Ozkara C et al (2013) Recessive loss of function of the neuronal ubiquitin hydrolase UCHL1 leads to early-onset progressive neurodegeneration. *Proc Natl Acad Sci U S A* 110(9):3489–3494. <https://doi.org/10.1073/pnas.1222732110>
56. Coulombe J, Gamage P, Gray MT et al (2014) Loss of UCHL1 promotes age-related degenerative changes in the enteric nervous system. *Front Aging Neurosci* 6:129. <https://doi.org/10.3389/fnagi.2014.00129>
57. Zhang Y, Huang X, Zhao XY, Hu YJ, Sun HY, Kong WJ (2017) Role of the ubiquitin C-terminal hydrolase L1-modulated ubiquitin proteasome system in auditory cortex senescence. *ORL J Otorhinolaryngol Relat Spec* 79(3):153–163. <https://doi.org/10.1159/000468944>
58. Wang X, Dong C, Sun L, Zhu L, Sun C, Ma R, Ning, Lu B et al (2016) Quantitative proteomic analysis of age-related subventricular zone proteins associated with neurodegenerative disease. *Sci Rep* 18(6):37443. <https://doi.org/10.1038/srep37443>
59. Chu KY, Li H, Wada K, Johnson JD (2012) Ubiquitin C-terminal hydrolase L1 is required for pancreatic beta cell survival and function in lipotoxic conditions. *Diabetologia* 55(1):128–140. <https://doi.org/10.1007/s00125-011-2323-1>
60. Reynolds JP, Jimenez-Mateos EM, Cao L, Bian F, Alves M, Miller-Delaney SF, Zhou A, Henshall DC (2017) Proteomic analysis after status epilepticus identifies UCHL1 as protective against hippocampal injury. *Neurochem Res* 10:2033–2054. <https://doi.org/10.1007/s11064-017-2260-6>
61. Zhang H, Luo W, Sun Y, Qiao Y, Zhang L, Zhao Z, Lv S (2016) Wnt/beta-catenin signaling mediated-UCH-L1 expression in podocytes of diabetic nephropathy. *Int J Mol Sci* 25(17):9. <https://doi.org/10.3390/ijms17091404>
62. Bedekovics T, Hussain S, Feldman AL et al (2016) UCH-L1 is induced in germinal center B cells and identifies patients with aggressive germinal center diffuse large B-cell lymphoma. *Blood* 127(12):1564–1574. <https://doi.org/10.1182/blood-2015-07-656678>

63. Kim HJ, Kim YM, Lim S et al (2009) Ubiquitin C-terminal hydrolase-L1 is a key regulator of tumor cell invasion and metastasis. *Oncogene* 28(1):117–127. <https://doi.org/10.1038/onc.2008.364>
64. Yan C, Huo H, Yang C et al (2018) Ubiquitin C-Terminal Hydrolase L1 regulates autophagy by inhibiting autophagosome formation through its deubiquitinating enzyme activity. *Biochem Biophys Res Commun* 497(2):726–733. <https://doi.org/10.1016/j.bbrc.2018.02.140>
65. Ummanni R, Jost E, Braig M, Lohmann F, Mundt F, Barrett C, Schlomm T, Sauter G et al (2011) Ubiquitin carboxyl-terminal hydrolase 1 (UCHL1) is a potential tumour suppressor in prostate cancer and is frequently silenced by promoter methylation. *Mol Cancer* 14(10):129. <https://doi.org/10.1186/1476-4598-10-129>
66. Goto Y, Zeng L, Yeom CJ, Zhu Y, Morinibu A, Shinomiya K, Kobayashi M, Hirota K et al (2015) UCHL1 provides diagnostic and antimetastatic strategies due to its deubiquitinating effect on HIF-1alpha. *Nat Commun* 23(6):6153. <https://doi.org/10.1038/ncomms7153>
67. Todi SV, Paulson HL (2011) Balancing act: deubiquitinating enzymes in the nervous system. *Trends Neurosci* 34(7):370–382. <https://doi.org/10.1016/j.tins.2011.05.004>
68. Wobst H, Forster S, Laurini C et al (2012) UCHL1 regulates ubiquitination and recycling of the neural cell adhesion molecule NCAM. *FEBS J* 279(23):4398–4409. <https://doi.org/10.1111/febs.12029>

Publisher's Note Springer Nature remains neutral with regard to jurisdictional claims in published maps and institutional affiliations.